Natural Hazards (2020) 101:995–1017
https://doi.org/10.1007/s11069-020-03906-z

ORIGINAL PAPER

Assessing the impact of topography and land cover data resolutions on two-dimensional HEC-RAS hydrodynamic model simulations for urban flood hazard analysis

Emrah Yalcin[1]

Received: 2 January 2020 / Accepted: 19 March 2020 / Published online: 28 March 2020

Abstract
This study assesses the effects of topography and land cover data resolutions on the estimates of flood extent, inundation depths, flow velocities, and arrival times of a two-dimensional (2D) hydrodynamic HEC-RAS model under differently sized mesh structures, with the example of the urban floodplain of Kilicozu Creek (Kirsehir, Turkey). To analyse these effects under a wide range of data conditions, seven different resolution digital surface models (DSMs) (from 0.0432 to 10 m/pixel) and Manning's roughness layers (MRLs) (from 2 to 25 m/pixel) are produced for the subject floodplain by processing the high-quality DSM and orthophoto of the Kirsehir city centre. Additionally, seven different computational point spacings (CPSs) (from 2 m × 2 m to 25 m × 25 m) are tested to evaluate changes in the model outputs depending on the dimensions of mesh grids. Simulations are carried out for 19 different DSM, MRL, and CPS configurations under the 500-year flood scenario. The simulation performed for the most detailed model configuration is utilised as the base model simulation to compare the performances of other simulations. The model simulation configurated with the 2 m cell size DSM, 10 m cell size MRL, and 10 m × 10 m CPS shows comparable performance to the base model simulation with a small loss in the accuracy of the estimates, indicating that very-fine-resolution (less than 2 m) topography and high-resolution (less than 10 m) land cover data may not be indispensable to produce reliable simulations with 2D urban flood modelling using HEC-RAS software.

Keywords 2D hydrodynamic modelling · Digital surface model · HEC-RAS · Kirsehir · Land cover map · Urban flooding

1 Introduction

Floods are among the most devastating natural hazards worldwide responsible for the tremendous loss of life and property over the past decades (Munich 2019). While it is not always possible to prevent flood events, their disastrous effects can be lessened significantly

✉ Emrah Yalcin
emrah.yalcin@ahievran.edu.tr

[1] Department of Civil Engineering, Kirsehir Ahi Evran University, 40100 Kirsehir, Turkey

if flood-prone areas are carefully identified in advance, and suitable risk management measures are put in place accordingly (Plate 2002). Understanding flooding processes in terms of flood extent, inundation depths, flow velocities, and arrival times is mandatory in developing effective risk mitigation strategies, especially for urban environments (Sahoo and Sreeja 2017). Records of past flood events gained from in situ observations or remote sensing platforms can guide in assessing risk areas in terms of depths and extent of flooding (Hagen and Lu 2011). However, numerical models are required to make more comprehensive analyses under possible future scenarios by considering also the dynamics of channel and floodplain flows (Quiroga et al. 2016; Lim and Brandt 2019).

There are several numerical models with different capabilities to perform one-dimensional (1D), two-dimensional (2D), 1D/2D coupled, and three-dimensional (3D) flooding simulations. Among these, 2D hydrodynamic models are seemed to be more appropriate in resolving complex inundation processes on large-scale urban landscapes due to their efficiency in simulating lateral unsteady flow dynamics, including backflow in floodplains (Merwade et al. 2008; Pinos and Timbe 2019). However, 2D modelling process and simulation results are affected by many sources of uncertainty (i.e. input data, model structure, and model parameters) that should be eliminated through calibration by using the detailed inundation data of some past events (Papaioannou et al. 2016). Because depth and velocity measurements associated with high flood events are unavailable in most cases, it may not be possible to calibrate the developed models and validate their simulation performances (Merwade et al. 2008).

The ability of an uncalibrated 2D flood routing model to produce reliable flood simulations mostly depends on the quality of inputted topography and surface roughness data and the level at which these data are captured in computational mesh structure (Merwade et al. 2008). These two key inputs to which 2D models exhibit high sensitivity are generally given in the form of digital surface model (DSM) and land cover raster, respectively. The availability of several DSM and land cover products from a variety of sources at a wide range of resolutions and significantly increasing acquisition cost as resolution increases make it difficult to select the optimal scales of input data that can stabilize model predictions. Hence, it is important to examine the impacts of varying the level of detail of input data on the responses of 2D hydrodynamic models. These examinations should be model based due to possible differences in data processing techniques applied by 2D models in assigning elevation and surface roughness values to computational mesh elements (Yalcin 2019a).

In many studies of the literature, the role of topography on 2D flood modelling has been discussed with focusing on inundation extent and depths by almost exclusively using DSMs with resolutions of 1 m or coarser (e.g. Sanders 2007; Cook and Merwade 2009; Bakula et al. 2016; Hsu et al. 2016; Vozinaki et al. 2017; Lim and Brandt 2019; Ogania et al. 2019). Little attention has been given to investigate the contribution of the use of submetre-scale DSMs in capturing complex flow patterns, especially on urban topographies (de Almeida et al. 2018). Moreover, the role of land cover data resolution in using distributed surface roughness characterisation based on land-use has received less attention (Liu et al. 2019). Past studies have mainly focused on the effects of assigned roughness coefficients in generating inundation extent and depths by considering two different uniform surface roughness values for channel and floodplain or a single uniform roughness value applicable for both channel and floodplain (e.g. Horritt and Bates 2002; Tayefi et al. 2007; Dimitriadis et al. 2016; Lim and Brandt 2019). Numerous single channel and single floodplain roughness value combinations or numerous uniform roughness values for entire flow area can be tested during the model calibration process to find out the most proper surface

roughness value pair or value that yields the best model performance. However, under the absence of past flood records required for model calibration, quantifying a representative uniform roughness characterisation is not an easy task, especially for densely urbanised floodplains. Considering the above gaps in the literature, a thorough understanding of the role played by topography and land cover data resolutions on the simulation performances of 2D models in terms of not only flood extent and flow depth estimates but also arrival time and flow velocity estimates of flood waters still needs to be investigated further.

The objective of this study is to assess the effects of topography and land cover data resolutions in simulating flood extent, inundation depths, flow velocities, and arrival times on an urban floodplain using a 2D hydrodynamic HEC-RAS model. HEC-RAS 5.0 software (US Army Corps of Engineers Institute for Water Resources Hydraulic Engineering Center, Davis, California) is selected for this assessment due to the popularity of its 1D version and foreseeing the preference potential of this new 2D version, released as public domain in 2016, for future flood studies (e.g. Farooq et al. 2019; Mihu-Pintilie et al. 2019; Rangari et al. 2019). The urban floodplain of Kilicozu Creek passing through the city centre of the Kirsehir province of Turkey is chosen as the case study area. To analyse the impacts of varying scales of input data under a wide range of data conditions and differently sized mesh structures, seven different resolution DSMs (from 0.0432 to 10 m/pixel) and land cover rasters (from 2 to 25 m/pixel) are tested considering seven different cell dimensions (from 2 m × 2 m to 25 m × 25 m) in constructing computational mesh structure. Under the lack of records of past flood events, spatial and statistical comparisons of the model simulations are made against the estimates of the most detailed model configuration established using the highest resolution input data and the mesh structure configured with the smallest cell dimension.

2 Study area

Kilicozu Creek is a branch of the Kizilirmak River and flows through the Central Anatolia Region of Turkey. The creek sources from the northern slopes of Baran Mountain (39°18′ N latitude and 33°48′ E longitude) and continues as a wide arc to the south, passing through the Kirsehir city centre, until it flows into the Kizilirmak River (38°59′ N latitude and 34°08′ E longitude). This stream drains an area of 563.51 km^2 along the 47 km flow route from its source to the Kirsehir city centre, as demonstrated in Fig. 1. The last major flood event from this catchment occurred in January 1966, resulting in the inundation of agricultural lands near the valley floor and severe damage of 41 buildings in the city (Sigal 2012). No records including flood hydrograph, flooding extent, and inundation depths are available for this event. Even if these records were available, they could not be used to ensure accuracy and reduce uncertainties of flood simulation outputs because of the major changes in the creek cross-section and in the floodplain topography.

In the year 1979, the natural creek sections passing through the urban region were changed to a rectangular channel, designed for the 500-year return period flood discharge of 120.1 m^3/s, to reduce inevitable flood impacts and improve drainage conditions in the city centre. In March 2014, the Kentpark recreation project, covering about 800 m of the channelized portion starting from the axis where the creek enters the city, was completed after 1.5 years of construction (Fig. 1). Within the scope of this project, instead of the rectangular channel having a 10 m × 3.5 m cross-section, a new channel was built in varying dimensions ranging from 10 to 88 m in width and from 1.30 and 4.71 m in depth (Sigal

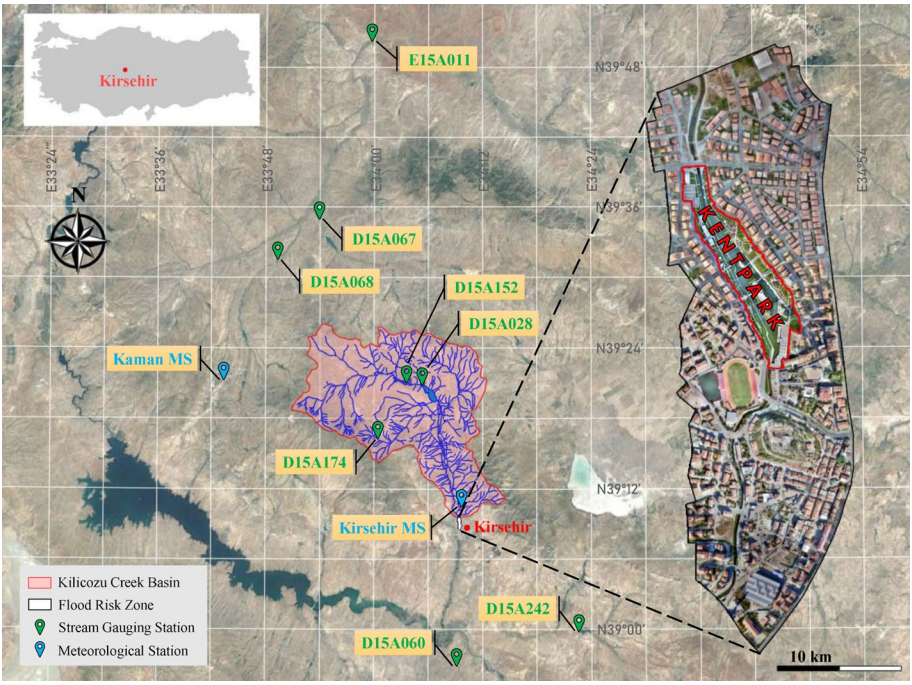

Fig. 1 Layout map of the study area

2012). In addition, two islands were located in the middle of the new channel section, and the sides of the channel were developed into a park with playgrounds, sports courts, social facilities, and stores. If the creek overflows from its channel in a possible flood event, the topography of the region may allow flood waters to spread out over an urbanised area of 1.08 km^2 with high pedestrian and vehicle traffic.

The design of the Kentpark project was based on the conducted simple open-channel computations considering the 500-year design discharge of the rectangular channel. Accordingly, the channel capacity of Kilicozu Creek was numerically evaluated to be adequate to carry a 500-year flood without overtopping (Sigal 2012). However, the validity of the used design discharge rate needs to be verified using the hydrological data observed during more than 40 years after the date of the discharge calculation. The re-estimation of this rate is also necessary to produce a flood hydrograph to be utilised in unsteady flood routing simulations. Through these simulations, the adequacy of the channel capacity can also be checked at the same time while assessing the effects of topography and land cover data qualities on the performance of 2D hydrodynamic HEC-RAS model.

3 Methodology

3.1 Generation of flooding scenario

The 500-year recurrence-interval flood scenario for the Kilicozu Creek basin is constituted through synthetic unit hydrograph methods and statistical analyses of runoff data.

The synthetic methods, namely, DSI, Snyder, and superposed Mockus, are applied using the annual maximum 24-h precipitation records of the Kirsehir and Kaman meteorological stations, shown in Fig. 1 (MGM 2018a). In the statistical estimation of flood peaks from observed runoff, the annual instantaneous maximum flow records of eight representative stream gauging stations, shown in Fig. 1, are utilised for regional flood frequency analysis (RFFA), and the station D15A152 is selected for point (or at-site) flood frequency analysis (PFFA) considering its drainage area and data quantity (DSI 2018). In these calculations, the upstream small-scale irrigation projects are not taken into consideration because there is no notable storage allocation for flood control in their reservoirs. The resultant hydrograph providing the highest flood discharges is utilised in the modelling part of the study to be on the safe side in assessing flood risk.

The derivation of synthetic hydrographs initiates with the calculation of the 500-year return period daily precipitation magnitudes of the Kirsehir and Kaman stations through the log-Pearson type 3 frequency distribution considering the Kolmogorov–Smirnov test statistics. The mean areal precipitation over the watershed is estimated using Thiessen polygons. The critical precipitation duration for the region is evaluated to be 4 h (Ozdemir 1978). Hence, the 500-year recurrence rainfall magnitude of the subject basin is determined by multiplying the mean areal precipitation with the 4-h pluviograph coefficient of the Kirsehir station, the 4-h areal distribution coefficient of rainfall of the basin, and a maximisation factor of 1.13 (Ozdemir 1978; Eren 2011). Next, the topographical parameters required in deriving synthetic unit hydrographs are measured on the 1:100,000 scale digitised topographic maps of the region. Substitution of these parameters into the synthetic methods gives 2-h unit hydrographs differing generally from each other in terms of peak discharge, time to peak discharge, and base time values. Then, for each method, the 500-year recurrence precipitation falling during the critical precipitation duration is subdivided into 2-h rainfall blocks using the appropriate regional time distribution curve of precipitation, and the SCS rainfall-runoff relationship is used to separate initial abstraction (i.e. interception and depression storages) and actual retention from rainfall and, hence, to estimate excess rainfall (or direct runoff) depth in each 2-h period (Ozdemir 1978; Ponce and Hawkins 1996; Usul 2017). Eventually, the synthetic flood hydrographs are obtained through the unit hydrograph method by using the 2-h synthetic unit hydrographs and the incremental excess rainfall depths, as presented in Fig. 2 (Ozdemir 1978; Dernek 2012).

To estimate flood hydrographs based on the regional flow data, the recurrence flood discharges of each stream gauging station are computed using the most appropriate frequency distribution function according to the Kolmogorov–Smirnov test. In PFFA, the 500-year return period flood peak of the station D15A152 is computed using the log-Pearson type 3 frequency distribution, as advised by Sarlak and Tigrek (2016), and brought to the basin outlet in proportional to the drainage areas. In RFFA, initially, a homogeneity test is applied for the determined base period concerning the observation periods of the considered gauging stations. After verifying the similarity of these stations, the non-dimensional 500-year recurrence flood peak of each station is calculated by dividing the 500-year recurrence flood discharge to the 2.33-year recurrence flood value. From the plotted curve of 2.33-year recurrence discharge versus drainage area, the 2.33-year recurrence flood value corresponding to the drainage area of the subject basin is read, and the 500-year return period regional flood peak is obtained by multiplying the read value with the mean value of the non-dimensional 500-year recurrence flood peaks of the gauging stations. Eventually, two more 500-year return period flood hydrographs are developed for the estimated flood peaks of PFFA and RFFA using the average unit hydrograph obtained by averaging the calculated 2-h synthetic unit hydrographs (Fig. 2).

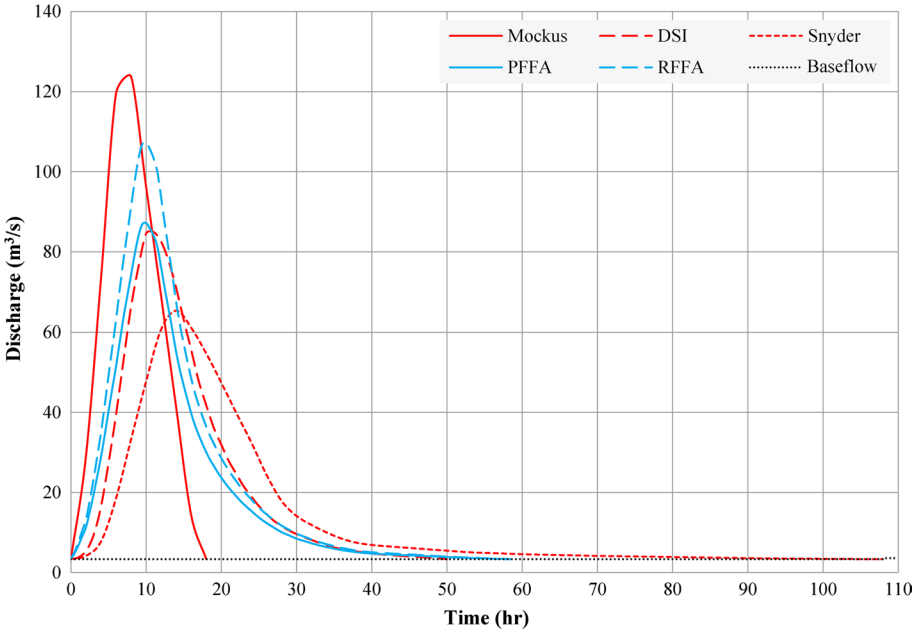

Fig. 2 The 500-year flood hydrographs

The baseflow of the Kilicozu basin is calculated by projecting the highest average flow value of the station D15A152 in the peak runoff period to the basin outlet in proportional to the drainage areas. The long-term snow-related statistics of the Kirsehir and Kaman meteorological stations demonstrate that a notable snowmelt contribution to runoff cannot be mentioned in the watershed (MGM 2018b). Hence, only a constant baseflow rate is added to the resultant flood hydrographs, as presented in Fig. 2. The flood hydrograph based on the Mockus method has the highest peak discharge of 123.8 m^3/s. This rate is almost equal to the 500-year recurrence flood peak of 120.1 m^3/s estimated by the Kayseri Regional Directorate of State Hydraulic Works and used directly as the design discharge of the Kentpark recreation project (Sigal 2012).

3.2 Generation of different resolution DSMs and land cover data

The base topographic data of the presumed flood-prone area of 1.08 km^2 is extracted from the high-resolution DSM generated using unmanned aerial vehicle (UAV)-based aerial photography to assess the flash flood risk in the Kirsehir city centre, as shown in Fig. 3a (Yalcin 2019b). The source DSM having a 4.32 cm/pixel ground sampling distance was produced by processing 2216 geo-referenced images acquired by the UAV flights over an area of 3.24 km^2 covering 60% of the city centre including the presumed floodplain of Kilicozu Creek. In image processing, 30 ground control points having known geographic positions were utilised for refining the geolocations of the acquired aerial images, and the absolute accuracy of the produced model was evaluated over the geodesic coordinates of three additional check points. Accordingly, the root mean square error values of this DSM

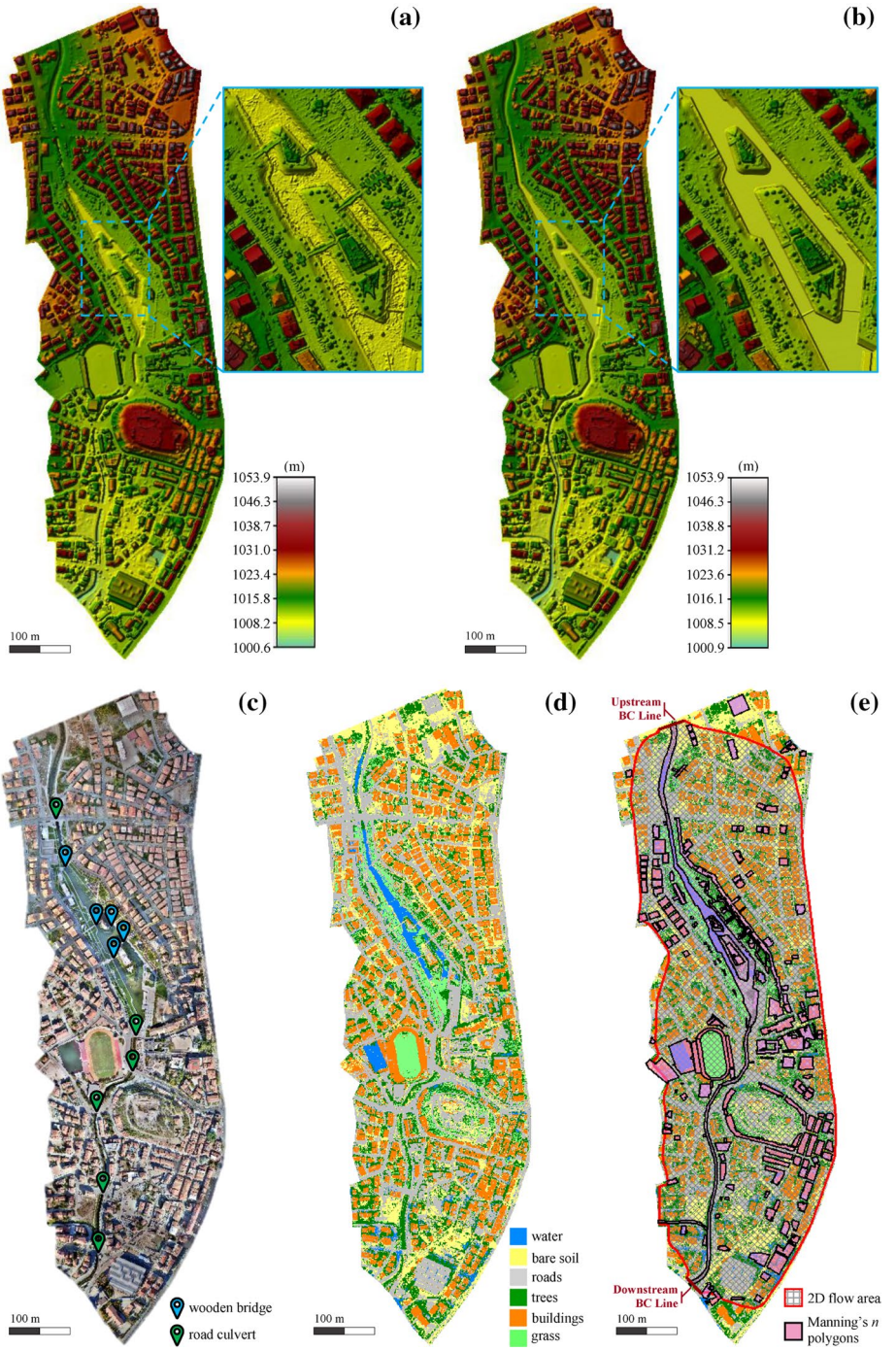

Fig. 3 DSM and land cover map generation process for the Kilicozu Creek floodplain: **a** unmodified DSM with 4.32 cm cell size, **b** modified DSM with 4.32 cm cell size, **c** orthophoto with the locations of the hydraulic structures, **d** classified land covers, **e** geometric data representation in HEC-RAS 5.0 software

were calculated as 5.1 and 12.7 cm for the horizontal and vertical planes, respectively (Yalcin 2018).

Before using the Kilicozu Creek portion of the source DSM in 2D hydrodynamic model analyses, the extracted DSM is modified for the existing hydraulic structures and the flow depths in the natural and channelized creek sections, as presented in Fig. 3b. There are six road culverts and five wooden pedestrian bridges on Kilicozu Creek, and the openings between their decks and bare ground appear as closed in the remote-sensed topographical data (Fig. 3a, c). After determining the dimensional and locational data of these structures, they are remodelled excluding their decks on the extracted terrain layer in the RAS Mapper interface of HEC-RAS 5.0 software. Next, the underwater bathymetry of the creek sections is merged with the terrain according to the construction drawings of the Kentpark recreation area and the terrestrial measurements. Then, pixel-sized voids in the resultant DSM caused by the terrain modifications are filled with the elevation void fill function in ArcGIS software (Environmental Systems Research Institute (ESRI), Redlands, California). The void-filled DSM having the same raster cell size of the source DSM is resampled to generate different resolution DSMs with 0.25, 0.50, 1, 2, 5, and 10 m cell sizes, as shown in Fig. 4a–f.

The orthophoto generated by integrating the geometrically corrected aerial images in Yalcin (2018) is utilised to classify land cover types in the subject area and, hence, to assign Manning's roughness (n) values for the classified land features. The portion of the orthophoto containing the Kilicozu Creek floodplain is extracted as presented in Fig. 3c, and the maximum likelihood classification tool of ArcGIS software is used to divide this combined image portion into six land classes as water, bare soil, roads, trees, buildings, and grass. The output cell size of the resulting raster data is set to 2 m considering the spatial distribution of land cover types across the region. As can be seen in Fig. 3d, there are several misclassifications, especially in building and water pixels of the produced land cover raster. In addition, it is near impossible to accurately distinguish channel pavement and the state of channel bed within water class using only the orthophoto. These misclassified regions need to be redefined manually in developing the 2D hydrodynamic model.

3.3 2D hydrodynamic modelling with different resolution DSMs and land cover classifications

Inundation simulations of the Kilicozu floodplain for the 500-year recurrence-interval flood scenario are conducted through a 2D hydrodynamic model developed in HEC-RAS 5.0 software (version 5.0.6). The effects of topography data on the model outputs, i.e. the extent of inundated area, inundation depths, flow velocities, and arrival times, are assessed by using the seven different resolution DSMs (0.0432, 0.25, 0.50, 1, 2, 5, and 10 m/pixel) of the subject floodplain. In the modelling process, after uploading the produced terrain rasters and orthophoto into the RAS Mapper interface of the software, a spatially varied Manning's roughness layer (MRL) is built by using the land cover raster formed with 2 m cell size. Additionally, to examine the effects of land cover data resolution on the simulation results, six more MRLs are developed by converting the cell size of the uploaded land cover raster in turn to 4, 6, 8, 10, 15, and 25 m in the same interface.

After building the terrain and roughness layers in RAS Mapper, the Manning's n values of 0.02, 0.03, 0.02, 0.06, 10, and 0.035 are assigned to the pre-defined water, bare soil, roads, trees, buildings, and grass classes, respectively, for each MRL in the geometric data editor of the software (Chow 1959). Based on the land cover data with 2 m/pixel

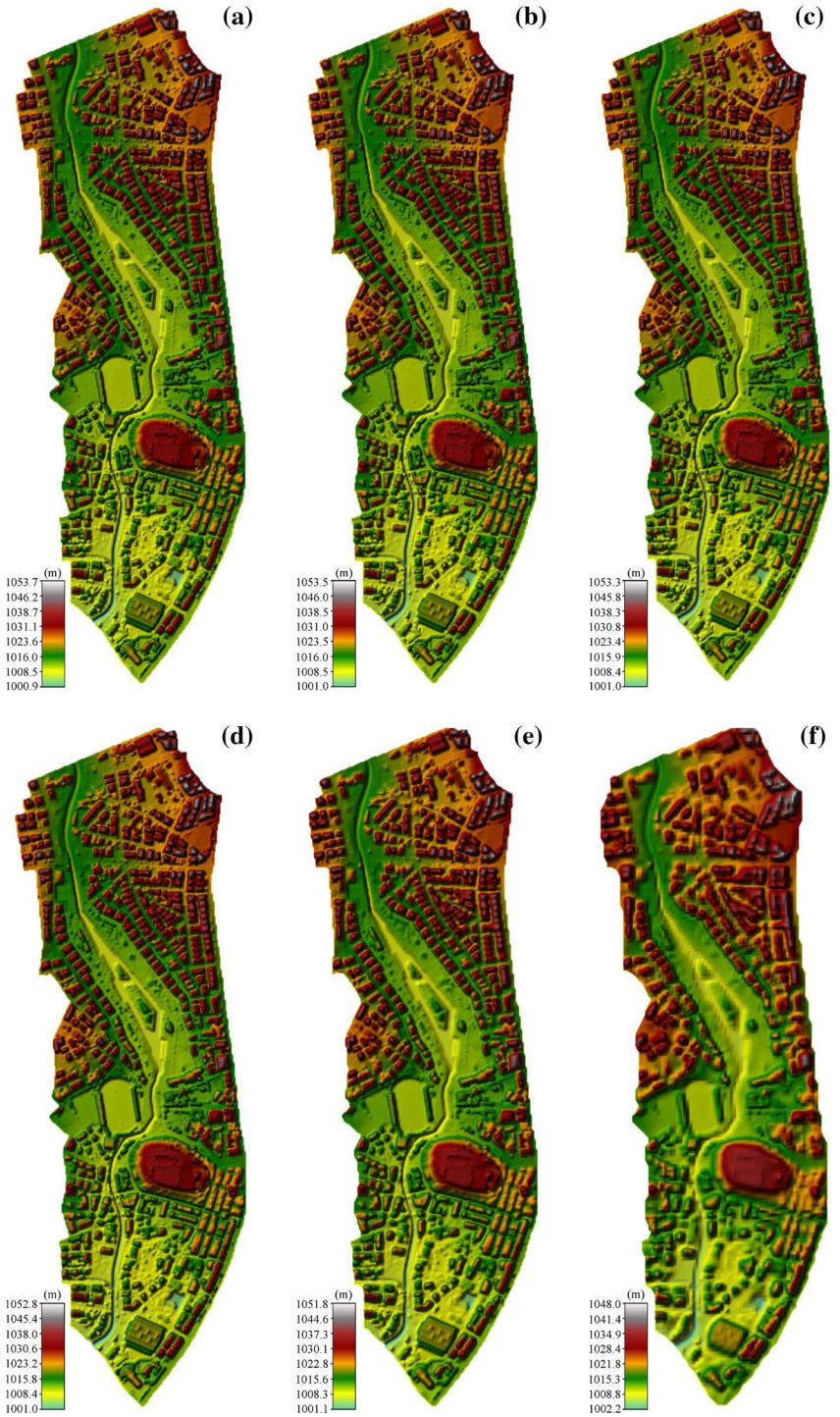

Fig. 4 DSMs of the Kilicozu Creek floodplain with **a** 0.25 m cell size, **b** 0.50 m cell size, **c** 1 m cell size, **d** 2 m cell size, **e** 5 m cell size, **f** 10 m cell size

resolution, the assigned n values of the misclassified regions are overridden by defining supplementary Manning's roughness polygons, as shown in Fig. 3e (Brunner and CEIWR-HEC 2016). Besides, all the water pixels identifying the streambed of Kilicozu Creek are redefined for the glazed tile-lined, concrete-lined with sides of cement rubble masonry, and natural creek sections by setting n coefficients to 0.015, 0.025, and 0.05, respectively (Chow 1959). The final state of the MRLs after all these reclassifications is presented in Fig. 5a–g.

A 2D flow area describing the boundary of the presumed flood domain is added by drawing a polygon by taking the orthophoto as the background layer in the geometric data editor of the software. Then, a computational mesh within the boundary layer is developed automatically with 2 m × 2 m computational point spacing (CPS), resulting in a total of 239,838 grid cells with an average size of 4.01 m^2 (Fig. 3e). Although this cell size is adequate to describe rapid changes in terrain and, therefore, in water surface slope, six more mesh configurations with 4 m × 4 m, 6 m × 6 m, 8 m × 8 m, 10 m × 10 m, 15 m × 15 m, and 25 m × 25 m CPSs are analysed to point out the effects of computational cell size on the model outputs and model run time. The numbers of grid cells in these mesh configurations are 59,812 (average cell size = 16.08 m^2), 26,514 (average cell size = 36.27 m^2), 14,873 (average cell size = 64.65 m^2), 9496 (average cell size = 101.26 m^2), 4192 (average cell size = 229.38 m^2), and 1486 (average cell size = 647.09 m^2), respectively.

The upstream and downstream ends of flooding are defined by drawing boundary condition (BC) lines along the outer boundary of the 2D area (Fig. 3e). The flow hydrograph and normal depth type BCs are utilised for putting flow into and taking flow out of the simulation domain, respectively. Within the unsteady flow data editor of the software, the ordinates of the resulting 500-year recurrence flood hydrograph with the highest peak discharge are inputted in 0.5-h time intervals by adding 1-h baseflow at the beginning and end of the base time of the flood hydrograph. The energy slope to be used in distributing flow along the upstream BC line for each computational time step is set based on the land slope in the vicinity of the upstream end of the overland flows. To define the normal depth type BC, the channel slope in the axis of the downstream BC line is entered as the friction slope to be used in calculating normal depths by Manning's equation (Brunner and CEIWR-HEC 2016).

Before performing model simulations, calculation options are specified within the unsteady flow analysis editor of the software. The diffusion wave equation option is set as the default for 2D unsteady flood routing within HEC-RAS. Although the other method, the full momentum (Saint–Venant) equation set, requires the use of a much smaller computation time interval and, therefore, a much higher run time than the diffusion wave method to run in a stable manner, the full momentum equation option is preferred to obtain more accurate simulation results (Brunner and CEIWR-HEC 2016). To avoid possible model stability issues, the computation time interval is assigned as 0.1 s considering the Courant–Friedrichs–Lewy condition (Courant et al. 1928; Brunner and CEIWR-HEC 2016). Besides, the initial conditions time option is used to ramp up the water surface from dry to wet condition within the 2D flow area. After performing several trial simulations, the total initial conditions time is set to be 1 h considering the travel time of the first flood wave between the two ends of flooding. One-half of this time (i.e. the first 30 min) is utilised for ramping up the external BCs to their initial values, and in the remaining time, the model is stabilised to a good initial condition throughout the entire 2D flow area (Brunner and CEIWR-HEC 2016).

Eventually, the 20-h flows of the 500-year flood scenario are simulated with a model output time interval of 1 min under 19 different DSM, CPS, and MRL configurations listed

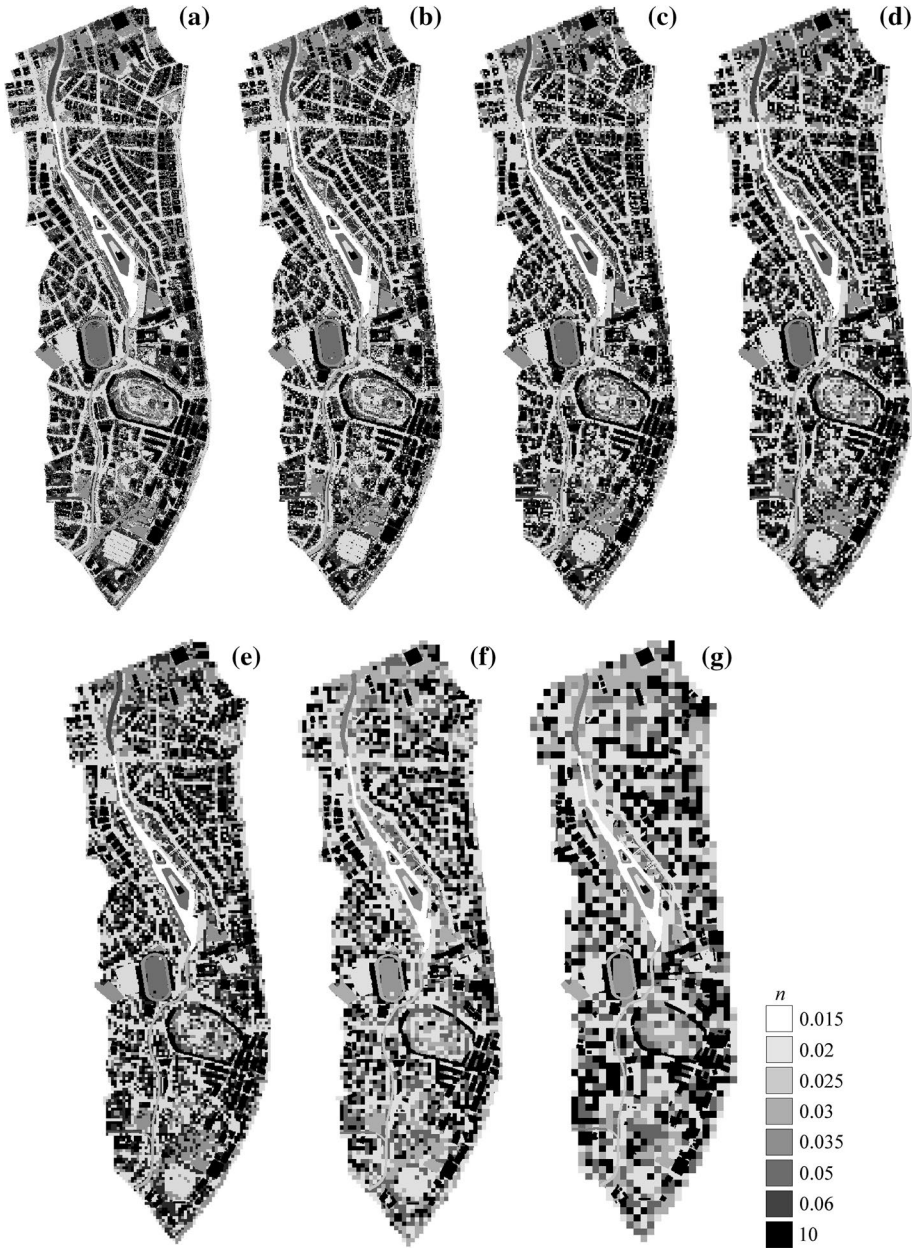

Fig. 5 MRLs of the Kilicozu Creek floodplain with **a** 2 m cell size, **b** 4 m cell size, **c** 6 m cell size, **d** 8 m cell size, **e** 10 m cell size, **f** 15 m cell size, **g** 25 m cell size

in Table 1. A base simulation (R1) is performed, initially, for the most detailed model configuration by the use of the 0.0432 m cell size DSM, 2 m × 2 m CPS, and 2 m cell size MRL. Then, three groups of simulations (R2–R7, R8–R13, and R14–R19) are carried out by setting up six different DSM, CPS, and MRL configurations for each of them without

Table 1 DSM, CPS, and MRL configurations of the model simulations and their run times

Simulation	DSM (m/pixel)	CPS (m × m)	MRL (m/pixel)	Model run time
Base simulation				
R1	0.0432	2 × 2	2	51 h:32 m
Simulations to assess the effects of topography data resolution				
R2	0.25	2 × 2	2	52 h:55 m
R3	0.5	2 × 2	2	52 h:15 m
R4	1	2 × 2	2	49 h:14 m
R5	2	2 × 2	2	51 h:44 m
R6	5	2 × 2	2	54 h:20 m
R7	10	2 × 2	2	51 h:13 m
Simulations to assess the effects of computational cell size				
R8	0.0432	4 × 4	2	12 h:48 m
R9	0.0432	6 × 6	2	6 h: 8 m
R10	0.0432	8 × 8	2	3 h: 37 m
R11	0.0432	10 × 10	2	2 h: 34 m
R12	0.0432	15 × 15	2	1 h: 3 m
R13	0.0432	25 × 25	2	22 m
Simulations to assess the effects of land cover data resolution				
R14	0.0432	4 × 4	4	12 h: 58 m
R15	0.0432	6 × 6	6	6 h: 19 m
R16	0.0432	8 × 8	8	3 h: 43 m
R17	0.0432	10 × 10	10	2 h: 31 m
R18	0.0432	15 × 15	15	59 m
R19	0.0432	25 × 25	25	21 m

changing any of the other model parameters to assess the effects of topography data resolution, computational cell size, and land cover data resolution on the model outputs through comparing with the base model simulation results. All model runs are conducted using the same Windows 10 (64 bit) notebook equipped with an Intel Core i7-6700HQ processor operating at 2.60 GHz, 16 GB memory, and a NVIDIA GeForce GTX 960 M graphics card, providing an opportunity to examine also the effects of the model configurations on simulation time.

4 Results and discussion

The outputs of the base simulation (R1), namely, flood extent, inundation depths, flow velocities, and arrival times, are demonstrated in a spatially distributed way on the orthophoto of the Kilicozu Creek floodplain in Fig. 6a–d, respectively. Accordingly, the results indicate that, contrary to the assertion in Sigal (2012), the channel capacity of Kilicozu Creek is not adequate to discharge waters of the subject catchment in a 500-year recurrence flood event. While overtopping occurs along almost all of the length of the channel, the most risk-prone zone of the whole floodplain is the surrounding regions of the Kentpark project where the inundation depths exceed 1 m. Although the arrival time of the flood

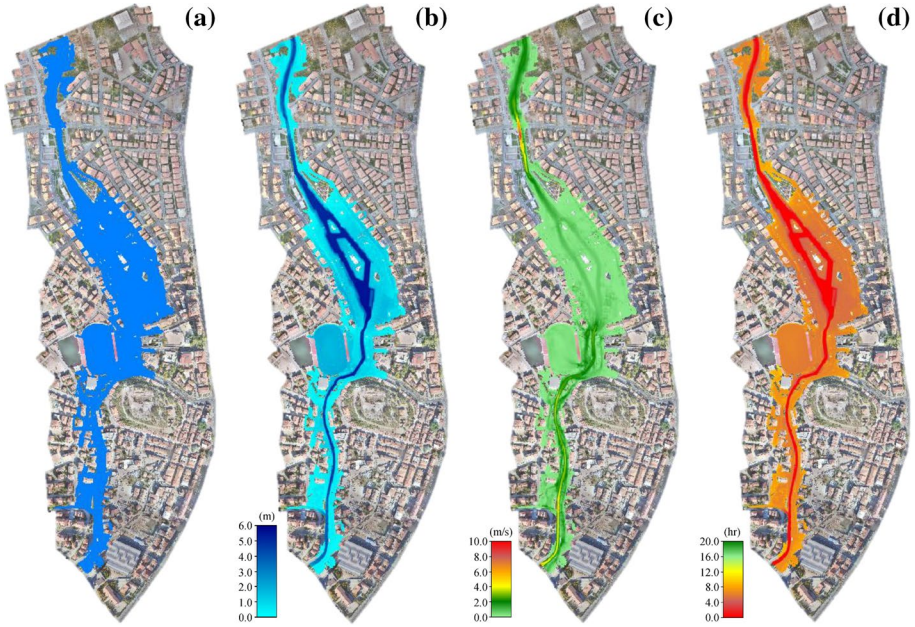

Fig. 6 Results of the base model simulation (R1): **a** flood extent, **b** inundation depths, **c** flow velocities, **d** arrival times

waters to the critical structures such as playgrounds, football stadium, social facilities, and stores is around 5 h after the start of the flooding, flow depths reach up to 2 m in this residential zone with intense pedestrian and vehicle traffic. On the other hand, no flow velocity of more than 1.5 m/s, faster than a person can escape, is detected within the extent of flooding (Dein 1985).

Although the 2D hydrodynamic model simulating lateral unsteady flow dynamics, including backflow in the floodplain, is much more reliable than the simple open-channel computations conducted for the design of the Kentpark project, these outputs cannot be relied upon alone without calibrating the model with observed flooding data (e.g. depths and velocities measured at different points). However, it is known that the ability of a 2D flood routing model to produce reliable estimates mostly depends on the quality of the used terrain data, assigned roughness values, and finite-element mesh configuration (Merwade et al. 2008). Hence, under the lack of records of past flood events, the use of a high-quality DSM (i.e. having centimetre-scale resolution and localisation accuracy) together with an adequate cell size for computational mesh and roughness layer in the R1 simulation seems to be sufficient to take this model configuration as the base model simulation in examining the effects of topography and land cover data resolutions under differently sized mesh structures on the model outputs.

The results of the R2–R19 simulations are compared with the ones of the R1 simulation spatially and statistically. The obtained inundation extents are analysed by superposing the output boundary polygons, and the percent error (PE) statistics of the inundation area estimates are used to evaluate the simulation performances. For the estimates of inundation depths, flow velocities, and arrival times, the difference tool of ArcGIS software is used to make pixel-over-pixel comparisons by computing the differences between the

output rasters (R1 minus R2–R19). In addition to these spatial comparisons, using the calculated pixel-based differences (i.e. errors), the performances of the R2–R19 simulations are evaluated against the R1 simulation in terms of the statistics of mean absolute error (MAE), standard deviation of errors (SDE), and root mean square error (RMSE). Moreover, to compare the effects of the model configurations on the model outputs having different scales, the ratio of RMSE to the standard deviation of the base simulation data (RSR) statistic is taken into consideration as a normalised dimensionless measure of RMSE. The results of these spatial and statistical analyses obtained in assessing the effects of topography data resolution, computational cell size, and land cover data resolution are presented in Figs. 7, 8, and 9, respectively.

By performing the first group of simulations (R2–R7) with the use of six different resolution DSMs (0.25, 0.50, 1, 2, 5, and 10 m/pixel) without changing the mesh configuration (2 m × 2 m CPS) and roughness data resolution (2 m cell size MRL), it is detected that the inundation areas of the R2–R7 simulations are quite close in size, shape, and spatial location to the extent of inundation in the R1 simulation although the boundary details reduce as the DSM resolution decreases (Fig. 7a–f). This similarity is not the case for the resultant inundation depths, flow velocities, and arrival times. No significant spatial differences in the estimates of flow dynamics are detected for the use of the DSMs having cell sizes up to 2 m although some local differences exist especially along the channel walls (Fig. 7a–d). However, the uses of the 5 m and 10 m cell size DSMs in the model configurations result in considerable increases of more than 0.5 m in the obtained inundation depths and non-negligible decreases of more than 1 h in the arrival time estimates over the entire extent of inundation, which would lead to inaccurate identification of flood risk areas. In addition, the differentiation in the obtained flow velocities for the channel sections becomes more pronounced by exceeding 0.5 m/s with the use of the 5 m and 10 m cell size DSMs (Fig. 7e, f). These findings are also evident from the deterioration in the MAE, SDE, RMSE, and RSR statistics of the R6 and R7 simulations compared to the statistics of the R2–R5 simulations (Fig. 7a–f). Moreover, the similarity of the RSR statistics calculated for the estimates of inundation depths, flow velocities, and arrival times with each other indicates that these model outputs are almost equally sensitive to the inputted DSM resolution.

To investigate the reason for the effects of decreased DSM resolution on the model outputs, the pixel-based elevation differences between the 0.0432 m cell size DSM and its lower-resolution versions are analysed spatially and statistically by using the difference tool of ArcGIS software. Accordingly, while the statistics of MAE, SDE, and RMSE are in turn as 0.37 m, 1.14 m, and 0.98 m for the 1 m cell size DSM, these error statistics increase logarithmically to 0.82 m, 2.06 m, and 1.75 m for the 2 m cell size DSM, respectively (Table 2). However, when these analyses conducted for the entire DEM area are repeated only to cover the inundation zone, it is observed that the statistics of MAE, SDE, and RMSE for the 2 m cell size DSM decrease in turn to 0.25 m, 0.63 m, and 0.55 m, as detailed in Table 3. The outputs of the first group of model simulations and the calculated elevation-error statistics of the lower-resolution DSM rasters show that DSM data having a resolution of at least 2 m/pixel are required to appropriately capture the topographical details of the analysed 2D flow area. In particular, a sufficient representation of the cross-sectional area of the rectangular channel sections (3.5 m in height and 10 m in width) is crucial due to the initiation of channel overtopping along these sections. As DSM resolution becomes lower, the cross-sectional area of this narrowest and longest part of the creek along the city passage decreases, resulting in increases in the obtained inundation depths and decreases in the arrival time estimates of flood waters over the entire extent of inundation (Fig. 7e, f).

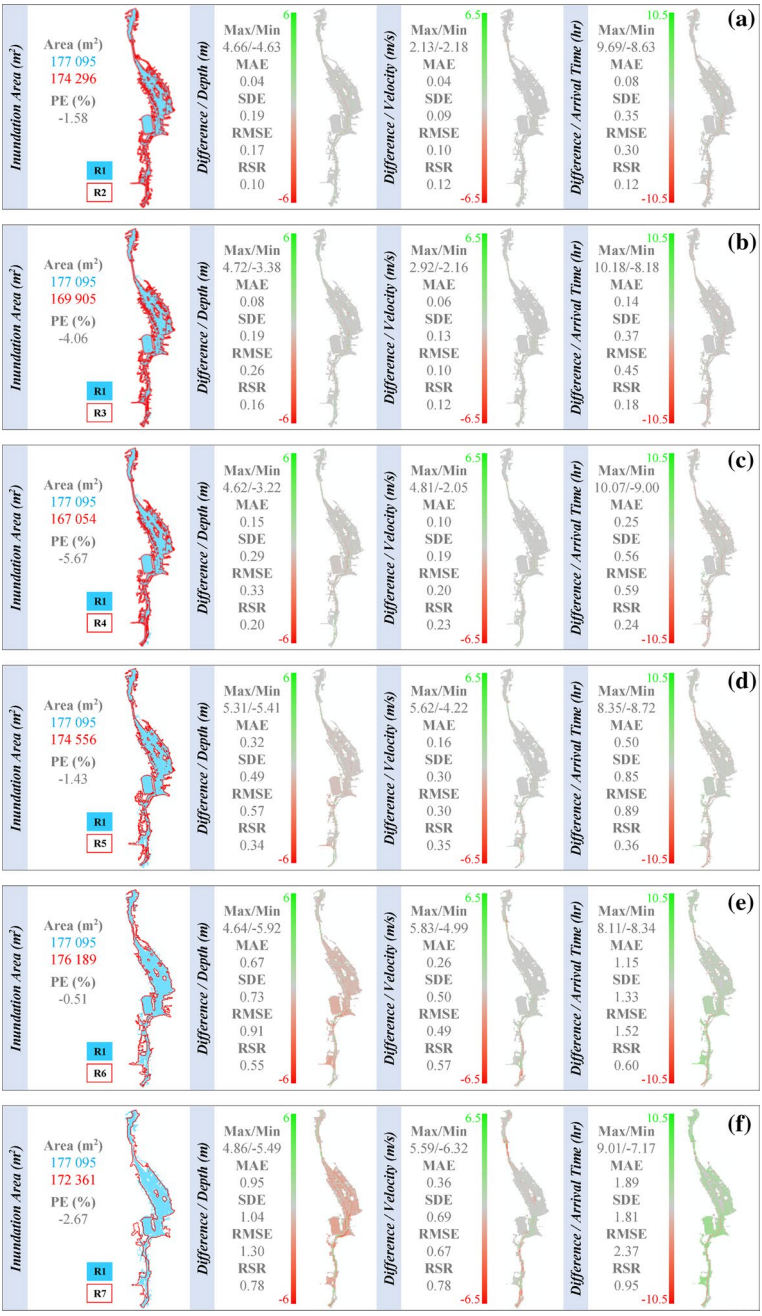

Fig. 7 Spatial and statistical analyses of the effects of topography data resolution on the simulated flood extent, inundation depths, flow velocities, and arrival times by comparing the R1 simulation with **a** the R2 simulation, **b** the R3 simulation, **c** the R4 simulation, **d** the R5 simulation, **e** the R6 simulation, **f** the R7 simulation

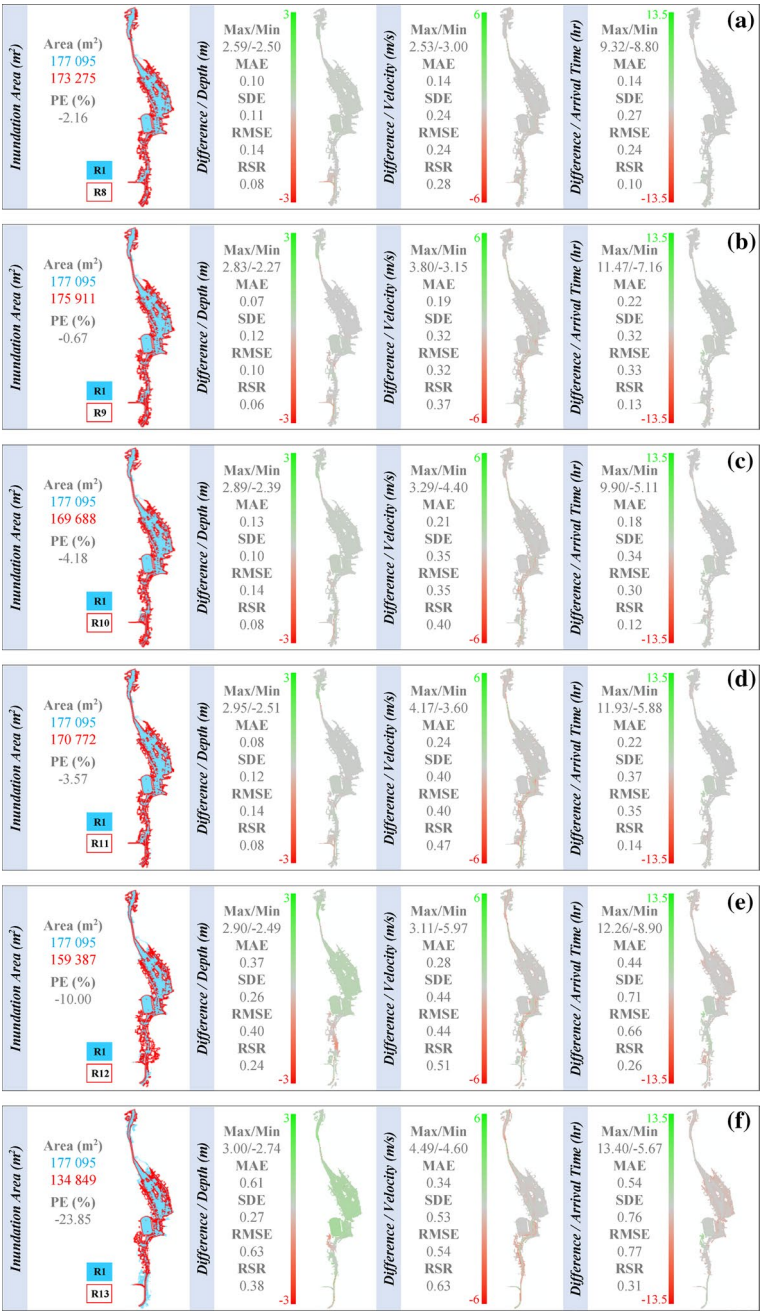

Fig. 8 Spatial and statistical analyses of the effects of computational cell size on the simulated flood extent, inundation depths, flow velocities, and arrival times by comparing the R1 simulation with **a** the R8 simulation, **b** the R9 simulation, **c** the R10 simulation, **d** the R11 simulation, **e** the R12 simulation, **f** the R13 simulation

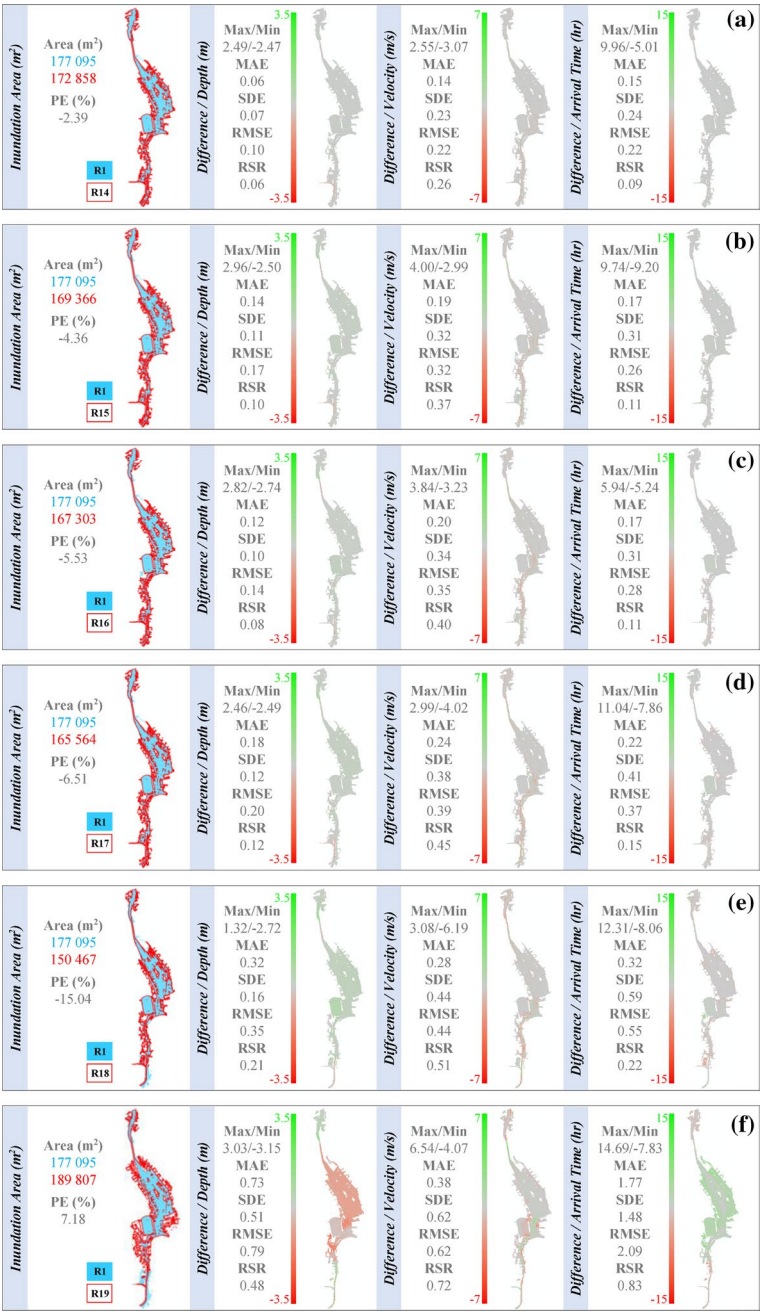

Fig. 9 Spatial and statistical analyses of the effects of land cover data resolution on the simulated flood extent, inundation depths, flow velocities, and arrival times by comparing the R1 simulation with **a** the R14 simulation, **b** the R15 simulation, **c** the R16 simulation, **d** the R17 simulation, **e** the R18 simulation, **f** the R19 simulation

Table 2 Statistical indices for comparison of the source DSM and the coarser-resolution DSMs

Difference	Max (m)	Min (m)	MAE (m)	SDE (m)	RMSE (m)
$DSM_{0.0432\ m/pixel} - DSM_{0.25\ m/pixel}$	22.23	−22.43	0.14	0.97	0.69
$DSM_{0.0432\ m/pixel} - DSM_{0.5\ m/pixel}$	16.91	−17.10	0.25	0.74	0.90
$DSM_{0.0432\ m/pixel} - DSM_{1\ m/pixel}$	18.13	−18.20	0.37	1.14	0.98
$DSM_{0.0432\ m/pixel} - DSM_{2\ m/pixel}$	24.00	−20.67	0.82	2.06	1.75
$DSM_{0.0432\ m/pixel} - DSM_{5\ m/pixel}$	22.13	−23.19	1.62	3.08	2.79
$DSM_{0.0432\ m/pixel} - DSM_{10\ m/pixel}$	24.06	−23.66	2.20	4.43	3.26

Table 3 Statistical indices for comparison of the source DSM and the coarser-resolution DSMs considering only the inundation zone

Difference	Max (m)	Min (m)	MAE (m)	SDE (m)	RMSE (m)
$DSM_{0.0432\ m/pixel} - DSM_{0.25\ m/pixel}$	18.44	−4.57	0.03	0.29	0.17
$DSM_{0.0432\ m/pixel} - DSM_{0.5\ m/pixel}$	13.02	−7.80	0.09	0.24	0.30
$DSM_{0.0432\ m/pixel} - DSM_{1\ m/pixel}$	12.01	−6.37	0.13	0.37	0.33
$DSM_{0.0432\ m/pixel} - DSM_{2\ m/pixel}$	13.91	−6.25	0.25	0.63	0.55
$DSM_{0.0432\ m/pixel} - DSM_{5\ m/pixel}$	18.06	−9.64	0.58	1.27	1.04
$DSM_{0.0432\ m/pixel} - DSM_{10\ m/pixel}$	21.68	−11.91	0.95	1.91	1.48

In the second group of simulations (R8–R13), the HEC-RAS model configurated with the 0.0432 m cell size DSM and 2 m cell size MRL is simulated under six different mesh configurations (4 m×4 m, 6 m×6 m, 8 m×8 m, 10 m×10 m, 15 m×15 m, and 25 m×25 m CPSs). Comparisons of the model outputs obtained from the R8–R13 simulations with the ones of the R1 simulation show that although the effects of the computational cell size on the estimates of flow dynamics are relatively limited, the uses of the 15 m×15 m and 25 m×25 m CPSs in configuring the 2D mesh structure lead to significant reductions of more than 10% in the inundation area estimate over such a densely settled floodplain. As seen in Fig. 8a–f, as the computational cells become coarser, there are slight gradual increases in the number and the magnitude of error pixels of the resultant flow dynamics and, hence, in their MAE, SDE, RMSE, and RSR statistics. However, while quite similar flood extents are detected in the R8–R11 simulations (Fig. 8a–d), the R12 and R13 simulations performed under much coarser mesh structures estimate the inundated area to be 10% and 24% less than the R1 simulation, meaning that 14 and 38 of the buildings likely to be inundated would not be classified as at-risk, respectively (Fig. 8e, f).

HEC-RAS pre-processes the inputted DSM and land cover rasters to create hydraulic property tables by developing detailed elevation-volume relationships for each cell and elevation-hydraulic property curves (elevation vs. area, wetted perimeter, and roughness) for each cell face. The cell-to-cell movement of water is controlled using the data in these tables, and all the details of the underlying terrain are taken into account in simulating the water storage and conveyance of each cell, regardless of the computational cell size (Brunner and CEIWR-HEC 2016). Furthermore, as seen in Table 1, the model run time is directly proportional to the number of computational cells, and increasing the cell dimensions linearly decreases the model run time. However, the R12 and R13 simulations show that there are still limitations to the use of computational cells that are too coarse to capture

rapid changes in terrain geometry and, therefore, in water surface slopes and velocities through such an urbanised region. As can be seen in the RSR values shown in Fig. 8a–f, the deterioration of the flow velocity estimates is more than twice that of the inundation depth and arrival time estimates.

In the data pre-processing stage, HEC-RAS assigns a single Manning roughness value to each cell face, taking into account the roughness data only at the cell face centre (Brunner and CEIWR-HEC 2016). To analyse the effects of MRL resolution on the model outputs, the second group of simulations are repeated through the third group of simulations (R14–R19) using the MRLs (4, 6, 8, 10, 15, and 25 m/pixel) having the same cell size as the assigned CPSs. Accordingly, it is seen that the use of a land cover layer having a smaller cell size than the computational cells does not contribute to the improvement in the model accuracy unless the size of the computational cells is too large to capture the land cover heterogeneity of the region (Figs. 8a–f, 9a–f). There are no noticeable spatial and statistical differences between the outputs of the R8–R12 simulations and their equivalents in the R14–R18 simulations indicating that increasing the MRL resolution degrades the simulation performance of the model (Figs. 8a–e, 9a–e). However, the use of the 25 m cell size MRL under a coarse-sized mesh structure developed with the 25 m × 25 m CPS for the R19 simulation causes more significant spatial changes in the resultant flood extent than those of the R13 simulation performed using the 2 m cell size MRL, which would lead to erroneous risk identification for 69 buildings (Figs. 8f, 9f). Moreover, considering the statistical indices for the comparison of the R1 and R19 simulations, it can be said that the differentiation in the estimates of flow dynamics exceeds the level that would lead to inaccurate identification of flood risk areas (i.e. 0.5 m for inundation depths, 0.5 m/s for flow velocities, and 1 h for arrival times) with the use of the 25 m cell size MRL (Fig. 9f). The results of the second and third groups of model simulations indicate that a land cover data resolution that not only makes sense with the computational cell size but also has the spatial accuracy needed for defining the roughness values should be selected to increase the simulation accuracy of the HEC-RAS model. Hence, to capture rapid changes in the terrain geometry and the land cover heterogeneity of the region, it is necessary to use at most 10 m × 10 m CPS for the 2D mesh structure and an MRL with a resolution of at least 10 m/pixel in configuring the HEC-RAS model.

These three groups of simulations performed under a wide range of data conditions reveal the need for the use of a DSM raster with a resolution of at least 2 m/pixel (R5), a 2D mesh structure constructed using maximum dimensions of 10 m × 10 m for CPS (R11), and a land cover data having a resolution of at least 10 m/pixel (R17) in the model configuration to obtain a comparable simulation performance to the R1 simulation in terms of the estimates of flood extent, inundation depths, flow velocities, and arrival times. For the simulations performed under these minimum input data resolutions and maximum grid dimensions (R5, R11 and R17), the obtained inundation areas are quite close in size, shape, and spatial location to the extent of inundation in the R1 simulation and the RSR statistics of all the resultant flow dynamics are less than 0.50, allowing to say that these simulations can be judged as satisfactory (Figs. 7d, 8d, 9d). However, the uses of the DSMs, CPSs, and MRLs having larger cell sizes than these values in configuring the HEC-RAS model result in significant spatial and statistical deterioration in the estimates of at least one of the model outputs which would have strong influences on the identification of flood risk (Figs. 7e, f, 8e, f, 9e, f). When the HEC-RAS model is re-simulated under a new model configuration (R20) by the use of the 2 m cell size DSM, 10 m × 10 m CPS and 10 m cell size MRL to analyse the combined effects of these cell sizes on the estimates of flood extent and flow dynamics, it is observed that a comparable performance to the R1 simulation can still be

achieved in terms of all the model outputs, as presented in Fig. 10. The areal difference between the estimated inundation extents in the R1 and R20 simulations is about 5%, and the number of buildings remaining in this error-zone is only seven (Fig. 10a). Likewise, the RSR statistics of the estimates of flow dynamics are determined to be less than 0.50 (Fig. 10b–d). Moreover, the use of the 10 m × 10 m CPS in constructing the 2D mesh structure reduces the model run time by about 95% compared to the R1 simulation.

5 Conclusions

This study investigates how topography and land cover data resolutions affect the simulations of a 2D hydrodynamic model developed in HEC-RAS 5.0 software for the urban floodplain of Kilicozu Creek, under differently sized mesh structures. The results of spatial and statistical analyses of the model simulations performed under different DSM, CPS, and MRL configurations can be summarised in three main points: (1) the use of DSMs having a resolution lower than 2 m/pixel deteriorates the estimates of flow dynamics to the extent that they would lead to inaccurate risk assessment; (2) coarse mesh structures developed with CPSs higher than 10 m × 10 m give rise to significant errors in the estimated inundation extent due to unable to capture rapid changes in the terrain geometry; (3) there is no point in using an MRL having a smaller cell size than the computational cells of the mesh structure to improve model accuracy unless the computational cells and, hence, distributed surface roughness characterisation are too coarse to capture the land cover heterogeneity of the region. It must be noted that these findings are specific for the subject floodplain and may vary for other sites according to differences in topography and land

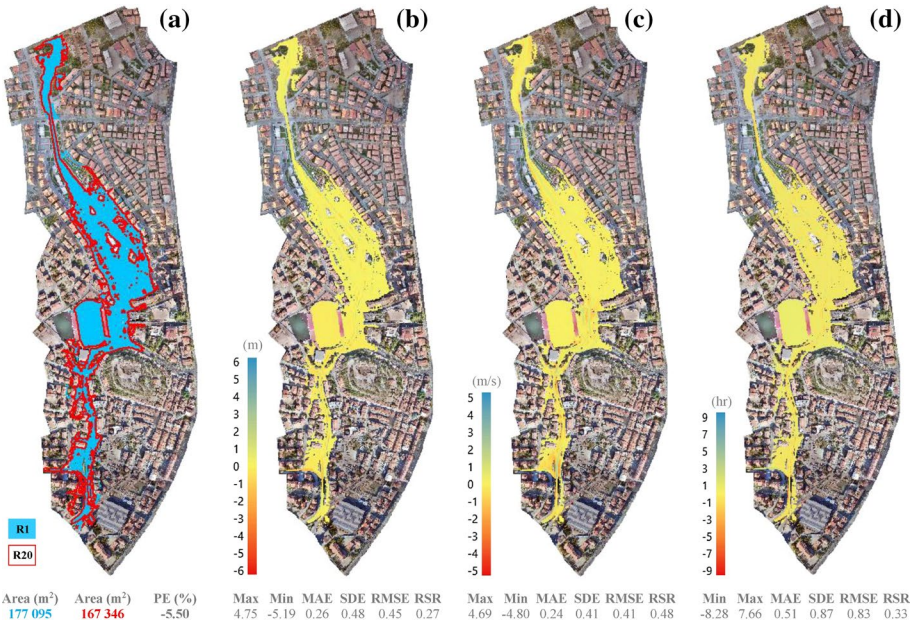

Fig. 10 Spatial and statistical comparison of the R1 simulation with the R20 simulation in terms of **a** flood extent, **b** inundation depths, **c** flow velocities, **d** arrival times

cover characteristics. However, the results are sufficient enough to conclude that very-fine-resolution (less than 2 m) topography and high-resolution (less than 10 m) land cover data may not be indispensable to produce reliable simulations with 2D urban flood modelling using HEC-RAS software.

Considering data acquisition cost and time efficiency, the determination of optimal scales of input data and mesh grids is crucial to produce reliable, but not undoubtedly accurate, flood simulations through a 2D flood routing model that cannot be calibrated due to the lack of records of past flood events. Although this assessment tries to answer the question of what should be the minimum DSM and land cover data resolutions in configuring an uncalibrated HEC-RAS model for reliably simulating an urban flood event, further studies on different floodplains with historical flood records are needed to investigate how uncalibrated HEC-RAS models should be configurated to obtain more accurate estimates of inundation extent and flow dynamics by considering also the sensitivity of the model to assigned surface roughness coefficients. In these studies, instead of using high-quality DSM and land cover rasters and their lower-resolution versions to analyse the model behaviour under a wide range of data conditions, it can be more useful to compare the products of different data sources such as satellite imagery, airborne light detection and ranging (LiDAR), aerial photography, and topographical maps. If such studies are also conducted for other 2D flood routing models, it will be possible to reach a general conclusion about which model should be preferred for available topographic and land cover datasets to perform more reliable and more accurate simulations in case of historical flood data scarcity.

Acknowledgements This work was supported by the Kirsehir Ahi Evran University Scientific Research Projects Coordination Unit (Grant No. MMF.A3.17.004). The UAV flight operations were conducted under the permission of the Governorship of Kirsehir (Permission No. 49249874.53197.(91244).2017).

References

Bakula K, Stepnik M, Kurczynski Z (2016) Influence of elevation data source on 2D hydraulic modelling. Acta Geophys 64(4):1176–1192. https://doi.org/10.1515/acgeo-2016-0030

Brunner GW, CEIWR-HEC (2016) HEC-RAS river analysis system, 2D modeling user's manual. US Army Corps of Engineers Institute for Water Resources Hydraulic Engineering Center, Davis

Chow VT (1959) Open channel hydraulics. McGraw-Hill, New York

Cook A, Merwade V (2009) Effect of topographic data, geometric configuration and modeling approach on flood inundation mapping. J Hydrol 377(1–2):131–142. https://doi.org/10.1016/j.jhydrol.2009.08.015

Courant R, Friedrichs K, Lewy H (1928) Über die partiellen Differenzengleichungen der mathematischen Physik. Math Ann 100(1):32–74. https://doi.org/10.1007/BF01448839

de Almeida GAM, Bates P, Ozdemir H (2018) Modelling urban floods at submetre resolution: challenges or opportunities for flood risk management? J Flood Risk Manag 11(S2):S855–S865. https://doi.org/10.1111/jfr3.12276

Dein MA (1985) Estimation of floods and recharge volumes in wadis Fatimah, Na'man and Turabah. Unpublished MSc thesis, King Abdulaziz University, Jeddah

Dernek E (2012) Design of overflow structures and example of Kayi River. MSc thesis, Namik Kemal University, Tekirdag (**in Turkish**)

Dimitriadis P, Tegos A, Oikonomou A, Pagana V, Koukouvinos A, Mamassis N, Koutsoyiannis D, Efstratiadis A (2016) Comparative evaluation of 1D and quasi-2D hydraulic models based on benchmark and real-world applications for uncertainty assessment in flood mapping. J Hydrol 534:478–492. https://doi.org/10.1016/j.jhydrol.2016.01.020

DSI (2018) Annual instantaneous maximum flows. General Directorate of State Hydraulic Works, Ankara

Eren ME (2011) Investigations on the flood risk of the Bogluca (Kayali) stream. MSc thesis, Yildiz Technical University, Istanbul (**in Turkish**)

Farooq M, Shafique M, Khattak MS (2019) Flood hazard assessment and mapping of River Swat using HEC-RAS 2D model and high-resolution 12-m TanDEM-X DEM (WorldDEM). Nat Hazards 97(2):477–492. https://doi.org/10.1007/s11069-019-03638-9

Hagen E, Lu XX (2011) Let us create flood hazard maps for developing countries. Nat Hazards 58(3):841–843. https://doi.org/10.1007/s11069-011-9750-7

Horritt MS, Bates PD (2002) Evaluation of 1D and 2D numerical models for predicting river flood inundation. J Hydrol 268(1–4):87–99. https://doi.org/10.1016/S0022-1694(02)00121-X

Hsu YC, Prinsen G, Bouaziz L, Lin YJ, Dahm R (2016) An investigation of DEM resolution influence on flood inundation simulation. Proc Eng 154:826–834. https://doi.org/10.1016/j.proeng.2016.07.435

Lim NJ, Brandt SA (2019) Flood map boundary sensitivity due to combined effects of DEM resolution and roughness in relation to model performance. Geom Nat Hazards Risk 10(1):1613–1647. https://doi.org/10.1080/19475705.2019.1604573

Liu Z, Merwade V, Jafarzadegan K (2019) Investigating the role of model structure and surface roughness in generating flood inundation extents using one- and two-dimensional hydraulic models. J Flood Risk Manag 12(1):e12347. https://doi.org/10.1111/jfr3.12347

Merwade V, Olivera F, Arabi M, Edleman S (2008) Uncertainty in flood inundation mapping: current issues and future directions. J Hydrol Eng 13(7):608–620. https://doi.org/10.1061/(ASCE)1084-0699(2008)13:7(608)

MGM (2018a) Annual maximum precipitation records in standard times for the Kirsehir and Kaman stations. Turkish State Meteorological Service, Ankara

MGM (2018b) Long-term all parameters bulletins for the Kirsehir and Kaman stations. Turkish State Meteorological Service, Ankara

Mihu-Pintilie A, Cimpianu CI, Stoleriu CC, Perez MN, Paveluc LE (2019) Using high-density LiDAR data and 2D streamflow hydraulic modeling to improve urban flood hazard maps: a HEC-RAS multi-scenario approach. Water 11(9):1832. https://doi.org/10.3390/w11091832

Munich RE (2019) NatCatSERVICE natural loss events worldwide 1980–2018. Munich Reinsurance Company. https://natcatservice.munichre.com. Accessed 11 June 2019

Ogania JL, Puno GR, Alivio MBT, Taylaran JMG (2019) Effect of digital elevation model's resolution in producing flood hazard maps. Glob J Environ Sci Manag 5(1):95–106. https://doi.org/10.22034/GJESM.2019.01.08

Ozdemir H (1978) Applied flood hydrology. General Directorate of State Hydraulic Works, Ankara **(in Turkish)**

Papaioannou G, Loukas A, Vasiliades L, Aronica GT (2016) Flood inundation mapping sensitivity to riverine spatial resolution and modelling approach. Nat Hazards 83(1):117–132. https://doi.org/10.1007/s11069-016-2382-1

Pinos J, Timbe L (2019) Performance assessment of two-dimensional hydraulic models for generation of flood inundation maps in mountain river basins. Water Sci Eng 12(1):11–18. https://doi.org/10.1016/j.wse.2019.03.001

Plate EJ (2002) Flood risk and flood management. J Hydrol 267(1–2):2–11. https://doi.org/10.1016/S0022-1694(02)00135-X

Ponce VM, Hawkins RH (1996) Runoff curve number: has it reached maturity? J Hydrol Eng 1(1):11–19. https://doi.org/10.1061/(ASCE)1084-0699(1996)1:1(11)

Quiroga VM, Kure S, Udo K, Mano A (2016) Application of 2D numerical simulation for the analysis of the February 2014 Bolivian Amazonia flood: application of the new HEC-RAS version 5. Ribagua 3(1):25–33. https://doi.org/10.1016/j.riba.2015.12.001

Rangari VA, Umamahesh NV, Bhatt CM (2019) Assessment of inundation risk in urban floods using HEC RAS 2D. Model Earth Syst Environ 5(4):1839–1851. https://doi.org/10.1007/s40808-019-00641-8

Sahoo SN, Sreeja P (2017) Development of flood inundation maps and quantification of flood risk in an urban catchment of Brahmaputra River. ASCE ASME J Risk Uncertain Eng Syst Part A Civ Eng 3(1):A4015001. https://doi.org/10.1061/AJRUA6.0000822

Sanders BF (2007) Evaluation of on-line DEMs for flood inundation modeling. Adv Water Resour 30(8):1831–1843. https://doi.org/10.1016/j.advwatres.2007.02.005

Sarlak N, Tigrek S (2016) Flood frequency analysis: case study of Göksu River and Kayraktepe Dam. J Fac Eng Archit 31(4):1095–1103. https://doi.org/10.17341/gummfd.79436

Sigal (2012) Description report on the infrastructure projects of the Kirsehir Kilicozu Creek recreation area. Sigal Engineering Trade and Industry Limited Company, Ankara **(in Turkish)**

Tayefi V, Lane SN, Hardy RJ, Yu D (2007) A comparison of one-and two-dimensional approaches to modelling flood inundation over complex upland floodplains. Hydrol Process 21(23):3190–3202. https://doi.org/10.1002/hyp.6523

Usul N (2017) Engineering hydrology. METU Press, Ankara

Vozinaki AEK, Morianou GG, Alexakis DD, Tsanis IK (2017) Comparing 1D and combined 1D/2D hydraulic simulations using high-resolution topographic data: a case study of the Koiliaris basin, Greece. Hydrol Sci J 62(4):642–656. https://doi.org/10.1080/02626667.2016.1255746

Yalcin E (2018) Generation of high-resolution digital surface models for urban flood modelling using UAV imagery. WIT Trans Ecol Environ 215:357–366. https://doi.org/10.2495/EID180321

Yalcin E (2019a) HEC-RAS 5.0 vs. FLO-2D: a model comparison for flood hazard estimation. In: Proceedings of the 4th Eurasian conference on civil and environmental engineering (ECOCEE), Istanbul

Yalcin E (2019b) Two-dimensional hydrodynamic modelling for urban flood risk assessment using unmanned aerial vehicle imagery: a case study of Kirsehir, Turkey. J Flood Risk Manag 12(S1):e12499. https://doi.org/10.1111/jfr3.12499